

Anisotropic electron-beam damage and the collapse of carbon nanotubes

Vincent H. Crespi, Nasreen G. Chopra, Marvin L. Cohen, A. Zettl, and Steven G. Louie
Department of Physics, University of California at Berkeley, Berkeley, California 94720
and Materials Sciences Division, Lawrence Berkeley National Laboratory, Berkeley, California 94720
(Received 15 April 1996)

Irradiation of multiwalled carbon nanotubes with the 800-keV electron beam of a transmission electron microscope induces anisotropic collapse of the nanotube. Tight-binding molecular-dynamics simulations of tube response following momentum transfer from large-angle electron-nuclear collisions reveal a strongly anisotropic threshold for atomic displacement. The theoretical displacement threshold for an impulse perpendicular to the local tangent plane of a single-walled tube is roughly half the damage threshold for impulses within the tangent plane. The electron beam preferentially damages the front and back of the nanotube, producing the observed anisotropic collapse perpendicular to the direction of the beam. The attraction of opposite faces of the inner wall then accelerates the collapse. [S0163-1829(96)04132-X]

The great strength anticipated for defect-free carbon nanotubes¹ motivates an exploration of structural failure modes of nanoscale carbon fibers. Nanotubes of sufficiently large inner diameter are unstable towards flattening,² with smaller flattened tubes metastable against inflation.³ This failure mode seems to be induced by mechanical deformation. A more dramatic structural failure can be induced by damaging the tubes with energetic particles. We analyze results for tube failure caused by irradiation with 800-keV electrons. The pattern of damage is strongly energy dependent and more importantly strongly anisotropic with implications for the controlled modification of irradiated nanotubes. In addition, these studies provide insight into the dynamics of fragmentary graphitic sheets, a regime of possible relevance to the synthesis conditions of both carbon nanotubes and fullerene structures.

Electron-beam damage proceeds by two paths: direct knock-on collisions of electrons with atomic nuclei and radiolytic atomic displacement mediated by beam-induced electronic excitations. Radiolytic damage is minimal in metals, semimetals, and small-gap semiconductors because beam-induced electronic excitations are generally not sufficiently localized to efficiently couple to the kinetic Hamiltonian of a single atom. Since all carbon nanotubes are either metals, semimetals, or small-band-gap semiconductors,⁴ the primary cause of carbon nanotube beam damage is expected to be knock-on collisions with atomic nuclei.

For energy transfers above ~ 20 eV the cross section for knock-on collisions between a beam electron and a carbon nucleus is a rapidly increasing function of the beam energy. At an accelerating voltage of ~ 200 keV the cross section for energy transfers greater than 40 eV is roughly 2 b.⁵ Carbon nanostructures are stable over relatively long periods of time in a 200-keV electron beam. At 300 keV the corresponding cross section is 5-b. Ugarte^{6,7} has shown that a prolonged exposure to a high-intensity 300-keV beam can transform amorphous carbon and angular graphitic particles into rounded carbon onions, possibly (in the case of angular particles) by the introduction of double pentagon-heptagon defects.⁸ In the present work we examine the results of irradiation of multiwalled carbon nanotubes with 800-keV elec-

trons from the Berkeley Atomic Resolution Microscope (JEOL-ARM 1000, resolution 1.6 Å) and analyze a new failure mode of carbon nanotubes.

Multiwalled carbon nanotubes were synthesized in a conventional arc discharge chamber and prepared for high-resolution transmission electron microscopy in a manner described previously.² The object of present study is an ill-fated 13-walled nanotube with an inner gap of ~ 2 nm. Figure 1(a) shows this tube after 10 s of exposure with a beam flux of $2 \times 10^5 e/nm^2s$. At this point the walls are well defined and the inner gap is nearly uniform. Figure 1(b) shows the same tube after 70 s of irradiation. The walls are wiggly but still clearly visible. More dramatically, the inner gap has contracted nearly uniformly to ~ 1 nm (white arrows) in width. The full video image reveals that collapse accelerates as the inner gap approaches the graphitic inter-wall distance. The maintenance of clear lattice fringes along the sides of the tube as the inner region collapses indicates that front and back of the tube are preferentially damaged: a uniformly damaged tube would amorphize and collapse simultaneously.

Figure 1(c) shows the sample after 100 s of irradiation. The central gap is fully collapsed and the sidewalls are beginning to amorphize. Fourier analysis of Figure 1(a) reveals a fringe spacing of 3.38 Å; similar fringe spacings are observed in Fourier transforms of subsequent images. A comparison of Figs. 1(a) and 1(c) shows that the width of the final collapsed structure is equal to the width of the initial tube minus the ~ 2 -nm inner gap. The continuous evolution and fidelity of the inner and outer walls during the process of collapse confirms that greatest beam damage occurs in the unresolved regions on the front and back of the tube, destroying the circumferential continuity and allowing collapse.

Two questions present themselves: why are the front and back of the nanotube damaged first and what is the mechanism of collapse? To explore the anisotropy of the damage pattern we performed tight-binding molecular-dynamics⁹ simulations of knock-on collisions. We chose a 210-atom, 24-Å-long section of (5,5) tube for the damage simulations. Tubes are indexed by the circumferential periodicity of the

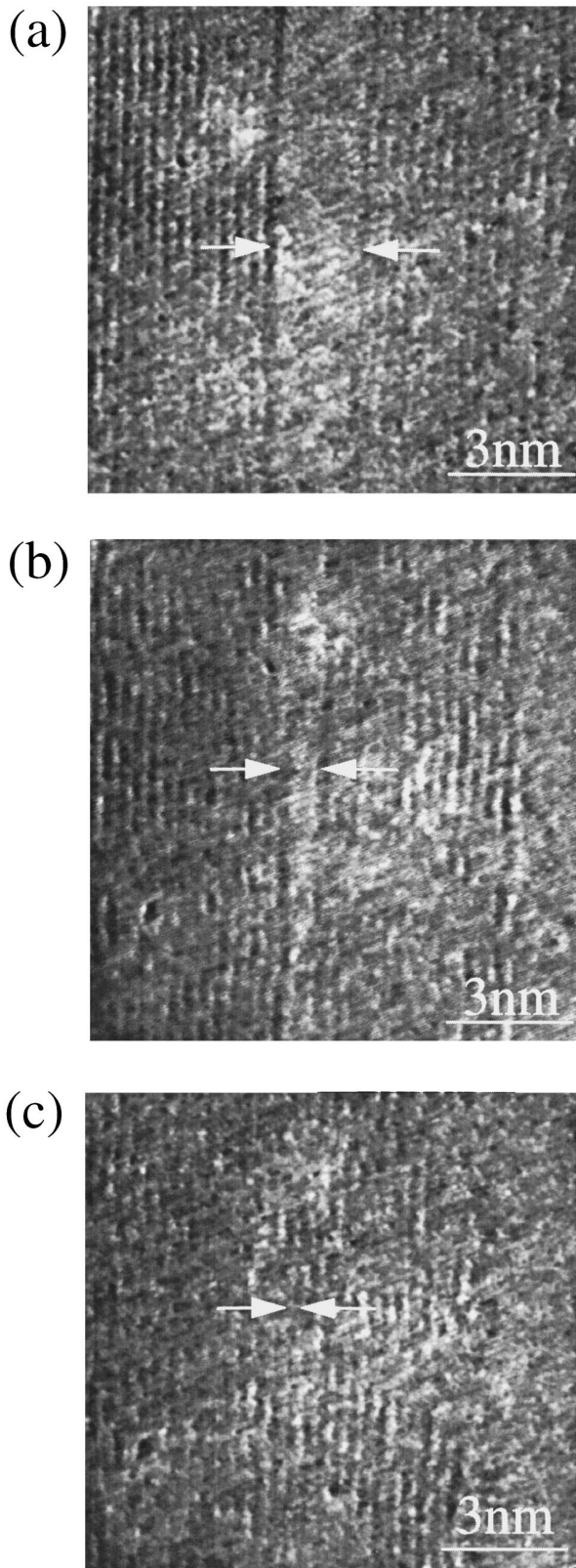


FIG. 1. Images from a video recording of a carbon nanotube collapsing under exposure to an 800-keV electron beam. (a) The 13-walled nanotube after 10 s of irradiation. The lattice planes of the individual walls are clearly visible. The arrows indicate the ~ 2 -nm central gap. (b) The same tube after 70 s. The lattice planes are only moderately perturbed, but the central gap has narrowed nearly uniformly to ~ 1 nm. (c) Complete collapse and the beginnings of amorphization after 100 s of irradiation.

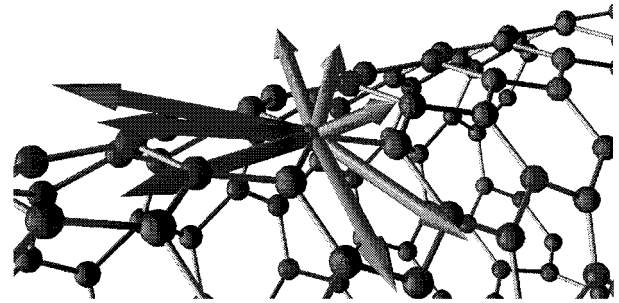


FIG. 2. Threshold escape energy from a (5,5) carbon nanotube as a function of the direction of initial impulse. The length of the arrows is proportional to the initial kinetic energy necessary for escape. Numerical values can be found in Table I.

equivalent graphite sheet following Saito *et al.*¹⁰ This tube section is small enough to allow efficient simulation and large enough to minimize finite-size effects (simulations on shorter tube sections reveal negligible differences in displacement thresholds). The choice of a nonchiral (5,5) tube allows easy separation of the effects of curvature from those of local bonding geometry. The scattered atom was chosen from the central region of the tube.

The calculated escape time of ~ 40 fs is large compared to the electronic response time of roughly $a/v \sim 4$ fs, with a the bond length and v a characteristic band velocity. Equivalently, the time-dependent electric field created by the escaping atom is too low in frequency to induce significant electronic transitions. The escape is therefore reasonably adiabatic and the tight-binding total-energy formalism is expected to be adequate.

The initial kinetic energy of the scattered atom was incremented in 2- or 3-eV steps until the atom escaped from the tube. Simulations continued for 60 fs, sufficient time for an escaping carbon atom with 1 eV of residual kinetic energy to travel ~ 2 Å far enough for a slow escape to be easily visible in the final atomic coordinates. The use of (2–3)-eV increments limits the precision of the displacement thresholds to a similar range. A finer increment is inappropriate since errors in the displacement energy caused by the use of a tight-binding parametrization are expected to be comparable.

For consistency, all damage simulations begin with the relaxed, undistorted zero-temperature structure. Although displacement thresholds in general can be temperature dependent, the high phonon frequency of carbon nanotubes argues against a strong temperature dependence to the displacement energy. Furthermore, the lack of Frenkel defects in the open graphitic nanotube structure minimizes temperature-dependent final-state effects. Finally, the relatively high thermal conductivity expected for carbon nanotubes should minimize the temperature increase expected from irradiation compared to other materials of similar aspect ratio and crystallinity. For completeness, we performed a finite-temperature escape simulation for escape at $\pi/4$ from the radial direction in a (5,5) nanotube at 1000 K. The escape energy was indistinguishable from the value obtained at $T=0$.

Figure 2 and Table I show the threshold for atomic ejection as a function of the direction of the impulse imparted to the scattered carbon atom. Impulses within the local tangent

TABLE I. Initial kinetic energy necessary for escape from an intact (5,5) carbon nanotube. Data are rendered graphically in Fig. 2. Tangential escape refers to initial impulses within the local tangent plane with $\theta=0$ referring to motion towards the nearest neighbor in the circumferential direction. Radial escape refers to initial impulses in a plane that slices circumferentially through the tube with $\theta=0$ referring to the radially outward direction. Uncertainties in displacement thresholds due to finite sampling of initial energies are ± 1 eV for integral thresholds and ± 1.5 eV for half-integral thresholds. Lower bounds correspond to directions where an interatomic distance during simulation falls below the range of validity of the simulation. For tangential angles of $\theta = \pi/4$ and $5\pi/6$ a dimer escapes.

θ	Displacement energy (eV)	
	Tangential	
0		>35
$\pi/4$		43.5
$\pi/3$		36
$\pi/2$		40.5
$3\pi/4$		>36
$5\pi/6$		41
π		33
	Radial	
0		17
$\pm \pi/4$		19
$-\pi$		19

plane cause large distortions of approximately ten neighboring atoms during the ejection process, which explains the large displacement threshold for these impulses. Impulses directly towards a nearest-neighbor atom reduced the interatomic distance below the range of validity of the dynamical simulation. We expect displacement thresholds for impulses towards neighboring atoms to equal or exceed those calculated for more computationally tractable directions. In contrast to tangential ejections, a radial impulse allows the atom to escape the tube with minimal distortion of the local environment. The 17-eV displacement threshold for escape in this direction is only moderately larger than the sum of the nearest-neighbor bond energies.

The variation in displacement threshold within the tangent plane can be decomposed into effects from curvature and local orientation. Angles of $\theta = \pi$ and $\pi/3$ describe escape opposite to the direction of a nearest neighbor. We attribute the 3-eV difference in displacement energy to tube curvature, since the smaller displacement energy at $\theta=0$ corresponds to the ejected atom traveling in the direction of greatest local curvature. The weak effect of wall curvature upon the escape energies suggests that the results for the (5,5) tube can be generalized to the exposed surfaces of larger tubes. Local orientation produces larger variations in tangential displacement energy. For example, escape at $\theta = \pi/3$ requires 36 eV, as compared to 43.5 eV for escape at $\theta = \pi/4$, a direction of

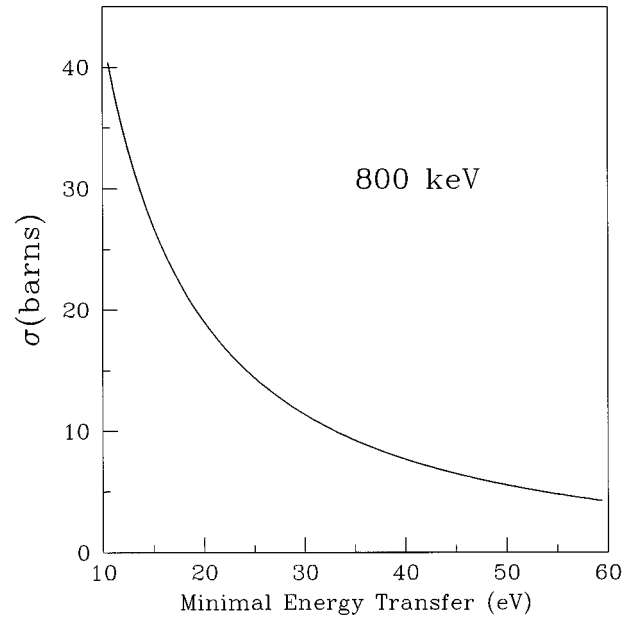


FIG. 3. Cross section for knock-on scattering of 800-keV electrons from a carbon nucleus. We show the integrated cross section for all scattering events imparting a nuclear kinetic energy greater than a minimal energy transfer.

greater local curvature, but also a direction more closely aligned with the nearest-neighbor bond. As mentioned previously, we expect impulses directed along the bonds to yield the largest displacement energies.

The difference between radial and tangential displacement energies is expected to increase slightly with increasing tube radius because impulses in the tangent plane are more nearly in the direction of neighboring atoms for a tube of small curvature. Therefore our results place a lower limit on the anisotropy in displacement energies for a larger tube.

In summary, ejection in the radial direction requires an energy transfer of ~ 17 eV, while tangential ejection requires an energy transfer of 30–50 eV. Scattering of 800-keV electrons off carbon nuclei at energy transfers greater than 10 eV yields a recoil velocity for the nucleus within a cone of maximum deviation $\pi/4$ from the beam direction with tighter collimation for higher-energy transfers. Figure 3 shows the scattering cross section as a function of the minimal kinetic energy transfer to the carbon nucleus.⁵ The cross section for energy transfers greater than 17 eV is three times the cross section for energy transfers greater than 40 eV. Since the nuclear recoil is directed in a narrow cone along the beam direction, our simulations indicate that knock-on displacement events are 2–3 times as common on the front and back sections of the tube as on the sides.

After moderate damage a significant fraction of the atoms remaining in the tube are located next to vacancies. The parallel and perpendicular displacement thresholds for atomic ejection near a vacancy are shown in Table II. Displacement thresholds for all directions are reduced, particularly for initial impulses in the tangent plane. The displacement threshold for impulses within the tangent plane is strongly anisotropic with atomic ejection easiest for impulses directed towards the vacancy. When ejected towards the vacancy the displaced atom can avoid the hard-core repulsive potential,

TABLE II. Initial kinetic energy necessary for escape from a site circumferentially adjacent to a vacancy in a (5,5) carbon nanotube. Tangential angles are measured relative to the direction of the missing atom. Definitions of terms are otherwise identical to Table I.

θ	Displacement energy (eV)	
	Tangential	
0		15
$\frac{\pi}{2}$		31
π		23
	Radial	
0		15

which induces large local distortions and produces the large displacement energies for tangential ejection from an undamaged local environment. Averaged over all tangential directions, the radial versus tangential displacement thresholds maintain a significant anisotropy after vacancy formation.

The preceding simulations were performed on a single-walled tube. The wealth of possibilities for intertube registry and vacancy location in combination with the large number of atoms to be simulated precludes an exhaustive series of molecular-dynamics simulations for atomic displacement in multiwalled nanotubes. To explore the effects of multiple walls we performed several simulations for ejection from the (5,5) inner wall of a double-walled nanotube with an (8,12) outer wall.¹¹ The definition of complete atomic ejection is problematic for ejection from the inner wall, since atomic motion is bounded by the outer wall.¹² We define ejection by the lack of local covalent bonding, whether sp , sp^2 , or sp^3 . Since exact damage thresholds depend on details of the intertube registry, we abstain from a detailed exposition and instead provide a semiquantitative overview. In the two-walled tube displacement energies for tangential impulses are increased by 5–10 eV over the single-walled values quoted in Table I. For predominately radial impulses, local sp^2 bonding is destroyed for low initial kinetic energies greater than 15 eV.¹³ Complete radial ejection is hindered by the outer wall, yielding displacement energies in the range 22–43 eV for initial impulses within $\pi/4$ of radially outward. Importantly, we discover that the hindering due to the outer wall is very sensitive to tube integrity. For example, adding a vacancy to the outer wall in the path of the ejected atom reduced the pure radial displacement energy from 43 ± 3 eV to 31 ± 1 eV. Unfortunately, complete characterization of this effect is computationally prohibitive. We note that the radiation damage of bulk graphite has been extensively studied in the context of nuclear reactor applications and the minimum kinetic-energy transfer with a significant probability of atomic displacement is measured to be ~ 30 eV,^{5,14} consistent with our tight-binding molecular-dynamics simulations of beam damage in multilayered locally graphitic structures.

These results for single- and multiple-walled tubes can be synthesized into a description of the initial stages of tube collapse. The most vulnerable portions of an irradiated nanotube¹⁵ are the exposed surfaces facing opposite to the beam direction (displacement energies 15–20 eV). After

moderate beam damage, the enhancement of damage threshold due to hindrance from these walls is reduced and the adjacent inner walls become similarly vulnerable. The region of most severe damage expands against the beam direction as the entire front and back of the tube are degraded while the sides suffer only moderate damage.

Having discussed the preferential damage to the front and back of an irradiated nanotube, we turn our attention to the mechanism of collapse. van der Waals and residual covalent interactions of either sp , sp^2 , or sp^3 character near the damage sites at the front and back of the tube pull the opposing inner edges of the damaged tube together. Collapse accelerates as the graphitic interwall distance of 3.4 Å is approached. Collapse in one portion increases the van der Waals and residual covalent attraction between the nearby opposing sections of inner wall, possibly inducing a zipper-like closure of the damaged nanotube reminiscent of that anticipated for a mechanically flattened nanotube.² This scenario is consistent with previous studies on the radiation damage of graphite that discovered a contraction of the basal plane (and dilation of the c axis) upon exposure to a beam fluence that displaces each atom approximately one time.¹⁶ Since the van der Waals attraction is beyond the tight-binding approximation (and the coordinates of a severely damaged nanotube are difficult to generate), this portion of the discussion is not amenable to dynamical simulation. The strong attraction of partially damaged and partially bonded graphitic sheets observed during tube collapse may help explain the exclusive production of multiwalled as opposed to single-walled carbon nanoscale structures in catalyst-free dc arc synthesis.

Electron channeling along crystallographic axes can drastically reduce the collisional cross section. However, channeling is very sensitive to alignment: misalignments of $\sim 1^\circ$ can destroy the effect.⁵ The curvature of a moderately sized multiwalled nanotube suggests that channeling effects are minimal for electrons incident perpendicular to the axis of the tube. We note that a significant reduction in collisional cross section should occur for a nanotube aligned axially with the beam.

The selective damage pattern could be exploited by irradiating with a beam capable of a maximal energy transfer just above the lowest damage thresholds, allowing controlled damage of exposed surfaces facing opposite the beam direction. The selective damage pattern of carbon nanotubes also suggests interesting failure modes for irradiated fullerenes.¹⁷ Novel final morphologies may be attained by careful radiation damage of crystallites of small fullerenes such as C_{60} . Finally, the anisotropic damage threshold has implications for the use of carbon nanostructures in radiatively hostile environments.

This research was supported by the Office of Naval Research, Order No. N0014-95-F-0099, by the National Science Foundation Grant No. DMR-9520554, and by the Office of Energy Research, Office of Basic Energy Sciences, Materials Sciences Division of the U. S. Department of Energy under Contract No. DE-AC03-76SF00098. N.G.C. acknowledges support from the Department of Education. A.Z. and S.G.L. acknowledge support from the Miller Institute for Basic Research in Science.

- ¹S. Iijima, *Nature* **354**, 56 (1991).
- ²N. G. Chopra, L. X. Benedict, V. H. Crespi, M. L. Cohen, S. G. Louie, and A. Zettl, *Nature* **377**, 135 (1995).
- ³L. X. Benedict, V. H. Crespi, N. G. Chopra, M. L. Cohen, S. G. Louie, and A. Zettl (unpublished.)
- ⁴N. Hamada, S. Sawada, and A. Oshiyama, *Phys. Rev. Lett.* **68**, 1579 (1992).
- ⁵L. W. Hobbs, in *Quantitative Electron Microscopy*, Vol. XXV of *NATO Advanced Study Institute, Series B: Physics*, edited by J. N. Chapman and A. J. Craven (Plenum, New York, 1984) p. 399.
- ⁶D. Ugarte, *Nature* **359**, 707 (1992).
- ⁷D. Ugarte, *Chem. Phys. Lett.* **207**, 473 (1993).
- ⁸We expect that sufficiently prolonged exposure to a 200-keV beam should induce similar changes in morphology.
- ⁹C. H. Xu, C. Z. Wang, C. T. Chan, and K. M. Ho, *J. Phys.-Condens. Matter* **4**, 6047 (1992).
- ¹⁰We use the naming convention of R. Saito, M. Fujita, G. Dresselhaus, and M. S. Dresselhaus, *Appl. Phys. Lett.* **60**, 2204 (1992).
- ¹¹The interwall spacing is $\sim 3.4 \text{ \AA}$.
- ¹²Recoil energies in excess of 50 eV may allow the ejected atom to penetrate the outer wall.
- ¹³Extended simulation of systems with these partially displaced atoms often results in recombination and healing of the original damage. Recombination after displacements into the interwall space should be less efficient in a partially damaged tube since the walls impinged upon would not have the structural integrity to restrict the motion of an ejected atom to the vicinity of the original site. Variations in interwall registry also affect the efficiency of rebound-enhanced recombination. Recombination in mutliwalled tubes appears to be more efficient for displacements caused by radial impulses, thereby suggesting an enhancement in damage anisotropy for single-walled nanotubes.
- ¹⁴R. F. Egerton, *Philos. Mag.* **35**, 1425 (1977);
- ¹⁵Strictly speaking, the most vulnerable portions of the nanotube are the exposed pentagon sites on the front and back of the tube end caps.
- ¹⁶B. T. Kelly, *Carbon* **15**, 117 (1977); D. F. Pedraza and J. Koike, *ibid.* **32**, 727 (1994); J. Koike and D. F. Pedraza, *J. Mater. Res.* **9**, 1899 (1994); K. Nakai, C. Kinoshita, and A. Matsunaga, *Ultramicroscopy* **39**, 361 (1991).
- ¹⁷S. Seraphin, S. Zhou, and J. Jiao, *J. Mater. Res.* **8**, 1895 (1993).